Applied Catalysis B: Environmental 183 (2016) 37–46

Contents lists available at ScienceDirect

Applied Catalysis B: Environmental

journal homepage: www.elsevier.com/locate/apcatb

Effect of GO phase in $Zn(OH)_2$/GO composite on the extent of photocatalytic reactive adsorption of mustard gas surrogate

Dimitrios A. Giannakoudakis[a,b], Javier A. Arcibar-Orozco[a], Teresa J. Bandosz[a,b,*]

[a] Department of Chemistry, The City College of New York, CUNY, 160 Convent Ave, New York, NY 10031, USA
[b] Ph.D Program un Chemistry, The Graduate Center of the City University of New York, 365 Fifth Avenue, New York, NY 10016, USA

ARTICLE INFO

Article history:
Received 10 June 2015
Received in revised form
14 September 2015
Accepted 6 October 2015
Available online 22 October 2015

Keywords:
Zinc hydroxide
Graphite oxide composites
2-Chloroethyl ethyl sulfide
Reactive adsorption
Mustard gas
Detoxification

ABSTRACT

Composites of zinc hydroxide with various contents of graphite oxide (GO) were synthesized with a controlled precipitation rate. They were used at ambient conditions as adsorbents of a mustard gas surrogate, 2-chloroethyl ethyl sulfide (CEES). The samples' surface features were characterized by various physical and chemical methods. The materials acted as photocatalysts upon light irradiation, degrading CEES to less- or no-toxic compounds. Exposure to visible light and the presence of GO in the composites improved the performance. The results indicated a paramount role of terminal OH groups as well as the porosity in the reactive adsorption process. The enhanced performance is linked to an increase in the degree of chemical and structural heterogeneity upon addition of GO. The surface characteristics strongly depend on the amount of the carbonaceous phase and 10 wt% was found as an optimal content. The CEES degraded mainly to ethyl vinyl sulfide by dehydrohalogenation and to hydroxyethyl ethyl sulfide via a hydrolysis pathway. The irradiation under visible light led to further transformation to vinyl vinyl sulfide and methyl vinyl sulfide through radical's reaction. The presence of GO promotes the electrons transfer and oxygen activation.

1. Introduction

One of the most widely used chemical warfare agents (CWA) is mustard gas also referred to as sulfur mustard (HD), which is a highly toxic blistering agent. Its toxicity to humans, similar to phosgene and hydrocyanic acid, is associated with the ability to alkylate proteins. It rapidly penetrates through a membrane into a living cell, releasing HCl after hydrolysis [1].

Because of the extremely high toxicity of HD, the simulant 2-chloroethyl ethyl sulfide or half mustard gas (CEES), which is less toxic, is often used for research studies focused on the development of decontamination technologies [2]. CEES contains the same $ClCH_2CH_2S$- group as HD does. This moiety is responsible for its toxicity. In general, the CEES degradation pathways can be through the cleavage of C—S or C—Cl bonds and through the photocatalytic degradation/oxidation, where hydroxyl radicals are usually the main oxidizing species [3].

Metal oxides/hydroxides are considered as suitable reactive/photoactive adsorbents for the catalytic decontamination of a variety of organic contaminants [4–6]. This is due to their large number of highly reactive terminal groups, thermal stability, enhanced reactivity, high surface area, and adsorption capability [7–9]. The efficiency of the catalytic and photocatalytic activity depends on a chemical nature, particle size, crystallinity and the surface area of a particular metal oxide/hydroxide.

There are studies on the adsorption of CWA or their surrogates on metal oxides, but mostly from solutions or by a direct contact of the materials with the liquid phase of CWA [10–15]. There are also some studies addressing CEES removal/deactivation from vapor phase. Mawhinney et al. studied in details the interactions of CEES with Al_2O_3 at different temperatures in a special IR cell [16,17]. Adsorption of CEES in N_2 atmosphere on carbon-coated porous magnesium oxide was studied by Vu et al. [18]. In all research where the adsorption from vapor phase was addressed, hydroxyl groups were indicated as playing a crucial role in surface interactions. Nevertheless, there are limited studies for the removal of vapors from the gas-phase at ambient conditions (ambient pressure, temperature and moisture content) [19,20]. Since those are the conditions of the potential use of CWA, there is a need for the research on the development of novel highly efficient and low cost materials, capable of totally detoxify CEES vapors. Employing photoactivity in visible light, in order to increase the efficiency of a catalytic degradation to less or nontoxic compounds, would be an advancement,

* Corresponding author at: Department of Chemistry, The City College of New York, CUNY, 160 Convent Ave, New York, NY 10031, USA. Fax: +1 212 650 6107.
E-mail address: tbandosz@ccny.cuny.edu (T.J. Bandosz).

http://dx.doi.org/10.1016/j.apcatb.2015.10.014
0926-3373/

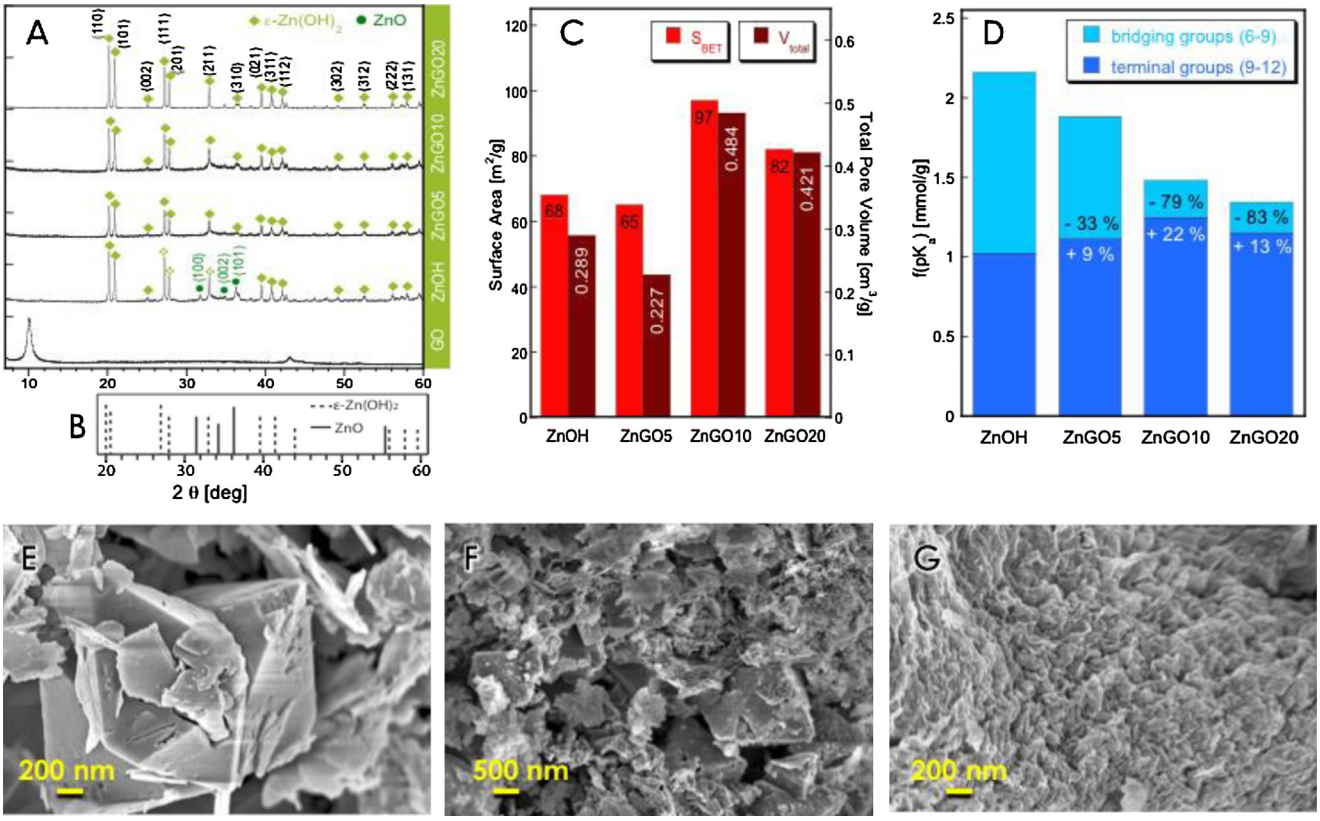

Fig. 1. X-ray diffraction patterns for the initial samples (A); JCPDS standard diffraction patterns for würtzite and wülfingite (B); parameters of porous structure calculated from the nitrogen adsorption isotherms (C); amounts of terminal OH groups detected from potentiometric titration experiments (D); SEM images of ZnOH (E); ZnGO5 (F) and ZnGO10 (G).

since 46% of the solar spectrum consists of irradiation in the visible light range [21].

Zinc oxides and hydroxide have attracted researchers' attention owing to their suitability for applications as gas sensors, varistors, in the fabrication of optical devises, and as gas adsorbents. As a well-known semiconductor, zinc (hydr) oxide has a wide band gap (3.0–3.3 eV) leading to the photoactivity in the visible range of violet spectrum (375.7–413.3 nm) [22–25]. Similar activity has been indicated for titanium dioxide (TiO_2) [26]. Upon exposure to visible light irradiation, both $Zn(OH)_2$ and TiO_2 can promote photocatalytic reactions, which can lead to the degradation of various organic pollutants [27–29].

It has been shown that zinc hydroxide, owing to the presence of OH groups, has a higher reactivity toward a CEES degradation in visible light than has zinc oxide [20]. An alteration in experimental conditions of sodium hydroxide addition to zinc chloride can lead to differences in the properties of precipitates [30,31]. The nucleation and growth of $Zn(OH)_2$ instead of ZnO is favorable at a low basicity (pH < 10) at room temperature, since the hydroxide phase is chemically and structurally stable [20,32]. At higher pH values, the hydroxide phase can be transformed to oxide [20,33].

Recent advances in materials science have led to the development of new efficient and photoactive adsorbents and catalysts containing graphene. It has been shown that the texture, the surface chemistry and the physicochemical properties of the metal oxide/hydroxide change dramatically after a GO addition [34–37]. Recently, the composites of zinc (hydr) oxide with graphite oxide have been reported as efficient reactive adsorbents of TICs such as H_2S [38,39] and SO_2 [40] at ambient conditions. The improvement in the performance was linked to an increase in the number of OH groups and in their surface dispersion. These groups were found to participate in oxidation reactions and in the formation of superoxide ions via the photochemical path with the contribution of a GO phase [41].

Based on the above, the objective of this paper is the evaluation of the composites consisting of GO and $Zn(OH)_2$ ($Zn(OH)_2$/GO) as photocatalytic reactive adsorbents with an intended application for CEES decomposition. The performance is studied under ambient light exposure, solar light irradiation (simulator) and in the dark. Since it was found that the high number of OH surface groups enhances the chemical reactivity [20], we target the composites with a increased amount of terminal active groups and with a higher surface area and total pore volume, compared to those of $Zn(OH)_2$. Moreover, the presence of GO may contribute to a faster electrons transfer and may improve oxygen activation. All of the aforementioned parameters would be of a paramount importance for the detoxification of CEES vapors.

2. Experimental

2.1. Materials

Zinc chloride ($ZnCl_2$) and sodium hydroxide (NaOH) with a purity higher than 99% and deionized water were used in this study. Graphite oxide (GO) was synthesized by oxidation of commercial graphite (Sigma-Aldrich) following the Hummers method [42]. Details of a GO preparation are presented elsewhere [39,43]. All materials were synthesized following a typical precipitation procedure at room temperature [20,38].

The composites of zinc hydroxide with GO were prepared by dispersing GO (5, 10 and 20% wt. of the final mass of the composite) in 0.5 L of a zinc chloride solution (0.05 M) and maintained under vigorous stirring for 2 h. Than the stoichiometric amount of NaOH (1L, 0.05 M) was added at a rate of 2.0 mL/min. The pH during synthesis

Table 1
Adsorption capacities measured at various conditions after one-day (1) exposure (L-exposure to ambient visible light, SL-exposure to solar light simulator; D-dark exposure).

	A_{ads} [mg/g]		
Sample	SL1	L1	D1
ZnOH	62	63	35
ZnGO5	79	77	38
ZnGO10	112	111	52
ZnGO20	87	88	43

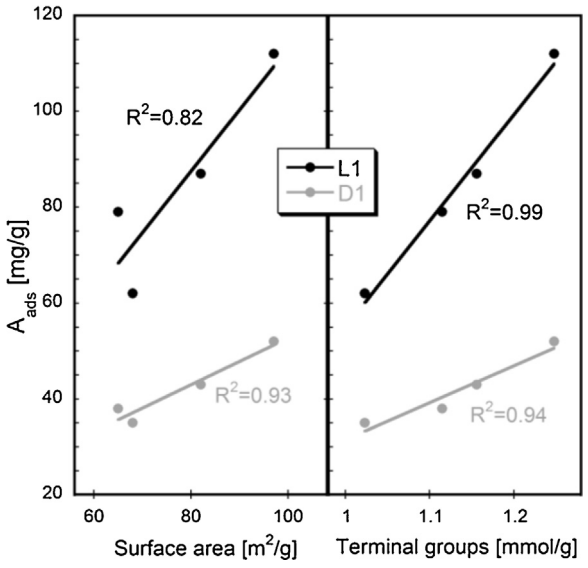

Fig. 2. Dependence of the amount adsorbed (after 24 h) on the surface area (left) and the terminal OH groups (right) under light exposure (L1) and in the dark (D1).

was maintained lower than 10, in order to avoid the transformation to zinc oxide [20]. The pH of the initial solution of $ZnCl_2$, with or without GO, was 5.8 ± 0.4. After the precipitation the final pH of all solutions remained less than 10 (9.3 ± 0.2). The obtained precipitate was filtered and then washed with deionized water until stable pH. Finally, the composites were dried at 60 °C for 48 h and they are referred to as ZnGO5, ZnGO10 and ZnGO20, where 5, 10 and 20 represent the content of GO in the composites, respectively. Zinc hydroxide was prepared following the same procedure as in the preparation of the composites without the addition of GO and it is referred to as ZnOH [20].

2.2. Methods

2.2.1. CEES reactive adsorption measurements

The reactive adsorption of CEES was carried out in batch experiments. Glass vial containing 20 mg of the selected sample was introduced into 22 mL reaction vessels, which were airtight closed with septa. 40 μL of CEES were injected through the septum into a second vial placed in the reaction vessel. The vessels were kept under ambient light exposure or under light from a solar light simulator (Xenon lamp, solar light Co., Inc., XPS-150^{TM}) or in the dark, at room temperature, for 1–9 days, depending on a target experiment. The vapor phases from the headspace of the containers were sampled with a syringe at the determined periods of time and injected to GC–MS. Then the containers were opened and the adsorbent samples were equilibrated for 1 h at atmospheric pressure, in the absence of moisture. Finally, the containers with the adsorbents were weighed and the increase in the weight was recorded. The experiments for all samples were run in parallel to ensure exactly the same ambient conditions (temperature and moisture contents) important for the performance comparison.

2.2.2. FT-IR spectroscopy

The Fourier transform infrared (FTIR) spectra were obtained in a Nicolet Magna-IR 830 spectrometer using the attenuated total reflectance (ATR) method. The spectrum was generated and collected 64 times in the wave range between 4000 and 600 cm^{-1} and corrected for the background noise.

2.2.3. X-ray diffraction (XRD)

Powder diffraction (XRD) patterns of as-synthesized grounded adsorbents were recorded using powder diffraction procedures on a Phillips X'Pert X-ray diffractometer, using a $Cu_{K\alpha}$ radiation (operated at 40 kV and 40 mA). The diffraction patterns were collected from 5 to 60 2θ at scan.

2.2.4. Thermal analysis (TA)

Thermogravimetric (TG) curves were obtained using a TA Instruments Thermal Analyzer (New Castle, DE, USA). The thermo gravimetrical (TG) and differential thermal (DTA) curves were obtained under a helium atmosphere (flow rate: 100 mL/min) with heating rate 10 °C per minute from room temperature to 1000 °C. The derivative thermograviemtric curves (DTG) were calculated from the TG curves.

2.2.5. Potentiometric titration

Potentiometric titration analyses were performed with an automatic titrator (888 Titrando, Metrohm). A suspension of 50 mg of the sample and 25 mL $NaNO_3$ (0.01 M) were added in a container and maintained at 25 °C overnight for equilibrium with continuous stirring. Throughout the entire titration procedure, the suspension was continuously saturated with N_2 to eliminate the influence of atmospheric CO_2 and stirred. Volumetric standard sodium hydroxide (0.1 M) was used as the titrant starting from the initial pH of the material suspension up to pH 11. The experimental data was transformed into a proton-binding curve, Q, representing the total number of protonated sites [44,45]. The SAIEUS procedure [45] used to deconvolute the proton-binding curves and the pK_a distributions for the species present on the surface were obtained.

2.2.6. Adsorption of nitrogen

Nitrogen isotherms were evaluated using an ASAP 2020 (Micromeritics) at −196 °C. The materials were outgassed at 120 °C to vacuum 10^{-4} Torr before the measurements. The Brunauer–Emmet–Teller method was used to calculate the surface area (S_{BET}). The micropore volume (V_{mic}, by using the Dubinin–Radushkevich approach), the mesopore volume (V_{mes}), the total pore volume (V_t, calculated from the last point of the isotherms based on the volume of nitrogen adsorbed) were calculated from the isotherms. The volume of mesopores, V_{mes}, represents the difference between the total pore volume and the micropore volume.

2.2.7. Scanning electron microscopy (SEM)

The morphology of the catalysts was observed with a Zeiss Supra 55 VP (accelerating voltage of 5.00 kV) and was performed in situ on the powder samples.

2.2.8. GC–MS analysis

Both CEES and its reaction products in the containers headspace were analyzed using a GC–MS QP5050A (Shimadzu). The separation of the compounds was performed in XTI-5 column (5% dephenyl-95% dimethyl polysiloxane) of 30 m length, 0.25 mm internal diameter, and 0.25 μm of liquid film thickness. The GC operation program was as follows: an increase from 50 °C to 100 °C

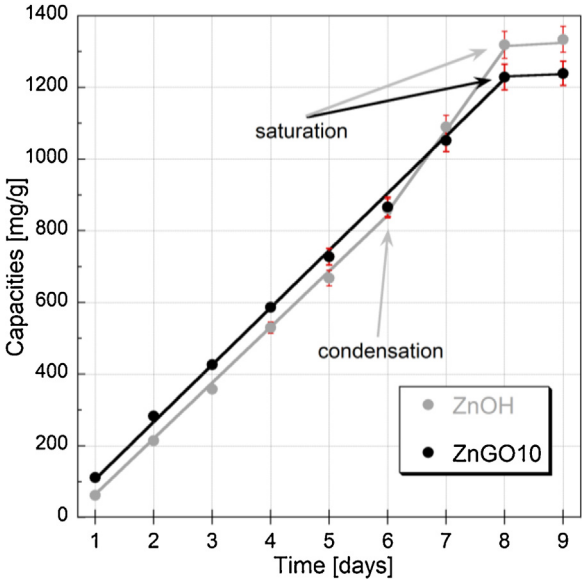

Fig. 3. Mass gains/adsorption capacities measured at visible light for up to nine days. The change in the slopes of lines indicates the change in the chemistry/physics of the interface (condensation of adsorbates on the surface and saturation).

at a rate of 5°/min, then the rate was changed to 40 °/min up to 280 °C. Helium was used as a carrier gas. The injection volume, total flow and the split ratio were 40 μL, 17.8 mL and 8, respectively. CEES was detected at the elusion time of 5.2 min, ethyl vinyl sulfide (EVS) at 1.9 min, vinyl vinyl sulfide (VVS) at 1.8 min and methyl vinyl sulfide (MVS) at 1.5 min. The mass spectrometer detector was used in an electron impact ionization mode. A calibration curve was prepared by adding 5, 10, 20 and 40 μL of CEES into the empty containers. After a complete evaporation of each volume of CEES, the areas of the peak at 5.1 min were used to prepare a calibration curve.

2.2.9. *Mass extraction and MS–MS analysis*

To qualitatively determine the byproducts of the CEES reactive adsorption, which are deposited on the materials' surfaces extraction with acetonitrile was carried out. 50 mg of the exhausted sample was equilibrated with 5 mL of the extracting agent for 5 days. Then, the solution was filtrated and injected into a mass spectrometry system (Q-TRAP 400, Applied Biosystems). The MS parameters used were as follows: ion spray voltage, 5500 V (highest sensibility); collision energy, from 10 to 50 V depending on the molecular weight selected; collision energy spread, 40 V, and declustering potential, 80 V. Nitrogen gas was used as a curtain and collision gas.

3. Results and discussion

Powder X-ray diffractograms of ZnOH and the composites (Fig. 1A) clearly indicate that the main crystallographic phase is ϵ-$Zn(OH)_2$. The diffraction peaks can be indexed as those of orthorhombic wülfingite (JCPDS 38-0385, Fig. 1B) [46]. However, the diffractogram of ZnOH revealed some minor diffraction peaks, which can be linked to a trace amount of hexagonal würtzite structure of zinc oxide (JCPDS 36-1451, Fig. 1B). These results are in agreement with our previous results focusing on zinc hydroxide and zinc oxide nanoparticles [20], although different batches of the materials were used in this study.

For the composites, no characteristic peaks of zinc oxide or of impurities were detected, confirming that a single-phase product was obtained. The characteristic peak corresponding to the d_{002} of GO at 10 2 θ was not detected, likely due to the exfoliation of this phase during the composite preparation. The average crystallite size was calculated using the Scherrer equation [47] from the (1 1 0) diffraction peak. While for ZnOH it is about 49.2 nm, for the composites the values of 35, 39 and 43 nm for 5, 10 and 20% of GO, respectively, were found.

Key factors known to affect the performance of adsorbents, especially for physical adsorption, are porosity and surface areas. The parameters of the porous structure calculated from the nitrogen adsorption isotherms are summarized in Fig. 1C. As seen, our synthesis approach leads to porous zinc hydroxide with a high surface area and volume of mesopores. The addition of the carbonaceous phase significantly increases the structural heterogeneity. 10% of GO results in the composite with the highest surface area and total pore volume, which increased 43 and 67%, respectively, comparing to those for ZnOH. The composite consisting of 5% GO shows a slight decrease in the surface area (−4%) and total porosity (−21%), in comparison to these parameters for ZnOH. ZnGO20 reveals higher porosity than that of ZnOH, but lower than that of ZnGO10. Apparently, there is an optimal amounts of GO resulting in the most pronounced porosity increase. Higher amount of GO can lead to limitations in the spatial growth of an inorganic phase.

The differences in surface chemistry of our materials are seen in the potentiometric titration results. The distributions of the groups on the surfaces of the composites differ from that of ZnOH (Fig. 1D). In general, bridging OH groups have pK_a range from 7 to 9 and OH terminal groups between 10 and 11.5 [48]. The amounts of the terminal OH groups increase for the composites, while the amounts of the bridging groups significantly decrease in comparison with those on the surface of ZnOH. ZnGO10 reveals the highest number of terminal groups with 22% raise comparing to those on ZnOH. In the case of ZnGO5, the changes are less pronounced.

The addition of the carbonaceous phase leads also to a higher ratio of the terminal to bridging OH groups (0.8 for ZnOH, 1.4 for ZnGO5, 5.0 for ZnGO10 and 5.6 for ZnGO20). The highest ratio is found for the composites with 10 and 20% GO. This can be linked to an increase in the dispersion and amorphicity level of zinc hydroxide upon the addition of GO. Moreover, the bridging groups could be involved in the formation of chemical bonds with the GO component [49].

The SEM image of ZnOH (Fig. 1E) shows the well crystallized ϵ-$Zn(OH)_2$ particles of a micrometric size with a bipyramid shape. Platelets-like particles of micron range size, which correspond to the zinc oxide phase, are found in a limited quantity. The addition of GO dramatically changes the crystal morphology. Zinc hydroxide particles of several tens of nanometers appear to surround the graphite oxide sheets, creating a web-like network with a high level of surface roughness [38,50]. For ZnGO5, the bipyramid shape of ϵ-$Zn(OH)_2$ particles are detectable (Fig. 1F). With an increase in the amount of GO, the zinc hydroxide particles are not detectable and the SEM images reveal the same surface morphology for the composites with 10 and 20% of GO (Fig. 1G).

The differences in the texture and chemistry of our samples are expected to affect the CEES reactive adsorption. An increase in the weight of the samples exposed to various periods of time (up to 9 days) was recorded. This increase represents the capacity (A_{ads}) of the materials to uptake CEES vapors and/or its surface reaction products [51]. It is considered that monitoring of the weight gained up to 9 days of the CEES exposure will provide a sufficient data on the kinetics and the mechanism of reactive adsorption.

The capacities after 24 h of the exposure are shown in Table 1. The vapor adsorption test was performed in ambient light (L1) and under a solar light simulator (SL1) in order to evaluate the role of the light intensity. Interestingly, the results showed that the usage of the solar light simulator did not alter the adsorption capacities for both materials. To evaluate the role of light, the adsorptions tests were also carried out in the dark.

The addition of GO results in larger weight gains for the composites than those for ZnOH, either under light or in the dark after the one-day exposure. These weight gains are apparent ones measured for the composites and not recalculated for the zinc hydroxide phase present in them. We consider these values as representing the final performance owing to the synergistic effect of composite formation. After exposure to ambient light or the solar light simulator for 24 h, ZnGO10 showed the best performance and the amount adsorbed on it was 81% higher in comparison to that on the zinc hydroxide sample. For the experiments performed in the dark this increase was less pronounced (49%). ZnGO5 showed the least increase comparing to the other composites (27% at light and 9% in the dark). On the other hand, on ZnGO20 the mass uptake was significantly higher comparing to that on ZnOH, but 22% smaller at light and 17% smaller in the dark than those of ZnGO10. This can be linked to the smaller amount of terminal hydroxyl groups, as well as to the decreased porosity compared to those for ZnGO10. The increased amounts adsorbed on the composites indicate that the graphene phase has a positive effect on the performance of these materials. It is important to mention that on pure GO no weight gain was recorded. The results show that there is a critical GO amount in the composite that provides a good decontamination performance.

The adsorption capacities of ZnOH in light showed a 77% increase compared to that measured in the dark. For the composites, this effect was more pronounced, since the light exposure increased the capacity more than two folds compared to those in the dark. This clearly indicates the relevant role of visible light in enhancing adsorption of CEES and/or its degradation products on the surface. This photocatalytic behavior is consistent with our previous findings, where zinc oxide and hydroxide were also photoactive under visible light toward CEES degradation [20].

In order to elucidate the role of surface features of our materials in the reactive adsorption process, the dependence between the adsorption capacity (A_{ads}) and the surface area (S_{BET}) or the number of the terminal hydroxyl groups was analyzed (Fig. 2). There is almost a linear trend in the dependence of the capacities measured at light and in the dark on the numbers of OH terminal groups with R^2 equal to 0.99 and 0.94, respectively. The dependence of the capacity, either in visible light or in the dark, on the surface area is slightly weaker and the correlation coefficients are 0.82 and 0.93, respectively. Nevertheless, the stronger correlation in visible light indicates the predominant role of terminal OH groups in the photoactivity of these materials. No correlation between the capacity and the number of bridging groups or the total pore volume was found.

The highest number of terminal hydroxyl group on ZnGO10, compared to all other samples, certainly plays a key role in the performance of this material. Another obvious reason might be related to an increase in the surface area and in the porosity upon the composite formation. Those two factors might be considered as linked to each other since a developed surface area and pore volume promote a favorable dispersion of the reactive adsorption centers. Similar conclusions on the involvement of the terminal OH groups of zinc hydroxide in CEES reactive adsorption were presented in our previous work [20].

Even though 24 h was an arbitrary time chosen for the adsorption/reaction process, we cannot cross out the hypothesis that slow reactions of CEES and of the compounds formed on the surface of the adsorbents are taking place for longer time. To study the extent of these processes affecting the kinetics of adsorption and influencing the degradation performance, the adsorption experiments were carried out for up to nine days. The increase in weight was observed until the ninth day. After that period of time no changes in A_{ads} were recorded. Both surface and headspace chemical compositions were analyzed. For these tests ZnOH and ZnGO10 were chosen because the results addressed above showed the latter sample as the best performing composite. Since the capacities measured using the solar simulator match those recorded at ambient light, the further discussion will focus on the results obtained at ambient light. Interestingly, the dependence of A_{ads} on the exposure time shows a linear trend with correlation coefficients 0.998 for ZnGO10 and 0.991 for ZnOH (Fig. 3). The mass gained on day 7 was almost equal to the initial mass of the samples (20 mg). This indicates that more than a half of the mass of the initially present CWA surrogate transfers to the adsorbents' surfaces. Until the sixth day, the uptake on the composite was higher than that on ZnOH. We link this to the higher dispersion of the active sites and thus to the higher degradation reactivity.

The adsorption results collected until the sixth day were fitted to the linearized-integral form of the Lagergren's pseudo-first order kinetic model. The plot of $\ln(q_e - q_t)$ vs t, where q_e is the maximum recorded capacity and q_t is the amount adsorbed at time t, shows straight lines with a high correlation coefficient R^2 (0.981 for ZnGO10 and 0.968 for ZnOH), suggesting that the adsorption behavior of CEES can be sufficiently described with the pseudo-first order model [52] until the eighth day. The results indicate that the adsorption rate is constant and not affected by the amount of the material.

After the sixth day, the mass gained on zinc hydroxide was higher than that on the composite. On the surface of the former sample, vapors started to condense and the color of the material changed from white to yellowish. Moreover, the sample began to resemble rather a gel than a solid matter and the mass gained occurred at a higher rate. The latter stopped with the saturation of the sample with condensed vapors (no change in weight recorded) on the ninth day. This condensation might be responsible for a change in the reactivity since the liquid layer on the surface of the sample will change the nature of interactions. The adsorption rates indicate that the samples are acting as catalysts until they get saturated with reactants. In the case of ZnGO10, the time needed to reach the saturation is longer than that for ZnOH and the condensation of vapors starts after the eight day. That delay in the surface condensation might be related to a higher catalytic activity of the composite than that of ZnOH. This can be linked to the higher pore volume, surface area and the number of terminal hydroxyl groups.

It is worth to mention that the maximum A_{ads} recorded on the ninth day was 1339 and 1236 mg/g for ZnOH and ZnGO10, respectively. The amounts adsorbed on the surface of ZnOH and ZnGO10 consist of 63% and 58% of the total initial mass of CEES, respectively. Since the initial amount of CEES totally evaporated and the maximum possible capacity would be 2120 mg/g (by assuming that the

Table 2
Details on the detected compounds on the surface and in the headspace.

Name	Linear formula	Abbreviation	Identification based on	Characteristic mass-to-charge ratio (m/z)
2-Chloroethyl ethyl sulfide	$CH_3CH_2SCH_2CH_2Cl$	CEES	TA–MS, GC–MS, MS–MS	124, 109, 89, 75, 61, 47
Ethyl vinyl sulfide	$CH_3CH_2SCH{=}CH_2$	EVS	TA–MS, GC–MS, MS–MS	88, 73, 60, 59, 45
2-Hydroxyethyl ethyl sulfide	$CH_3CH_2SCH_2CH_2OH$	HEES	TA–MS, MS–MS	106, 75, 61, 47
Vinyl vinyl sulfide	$CH_2{=}CHSCH{=}CH_2$	VVS	TA–MS, GC–MS	86, 85, 71, 59, 41, 40
Methyl vinyl sulfide	$CH_2{=}CHSCH_3$	MVS	TA–MS, GC–MS	74, 59, 47, 44, 40

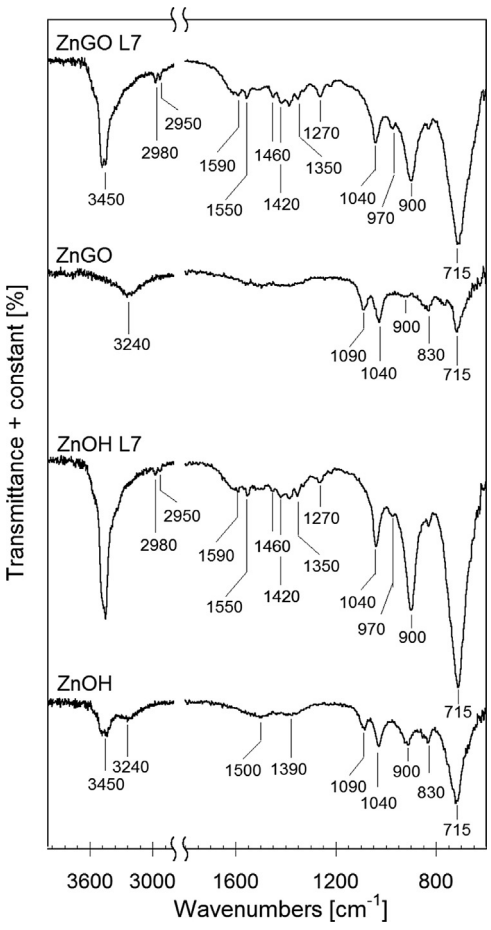

Fig. 4. FTIR spectra for the initial and exhausted samples after day 7 of CEES exposure.

entire amount of the CEES retained on the surface), the remaining mass of the CEES should remain unreacted or in a degraded state in the headspace.

The detected compounds on the surface and in the headspace along with their nomenclature, chemical formulas, abbreviations and the method used for their detection are listed in Table 2.

To analyze the species deposited on the surface of the adsorbents, FTIR spectra for the initial and the exhausted samples were analyzed. A comparison of the spectra for the initial and exhausted samples after 7 days of exposure in light is presented in Fig. 4. In the case of initial ZnOH, the bands at 715 and 900 cm^{-1} are assigned to the out-of-plane bending and vibration modes of the OH groups, while the bands observed at 830, 1040 and 1090 cm^{-1} are assigned to the deformation vibration of —OH groups, Zn—OH bending and —OH twisting vibration, respectively. The bands at 1390 cm^{-1} with a shoulder at 1360 cm^{-1}, and at 3450 cm^{-1} are assigned to the vibrations of OH groups coordinated to Zn(II) ions and the bands at 1500 cm^{-1} and at 3240 cm^{-1} to OH groups of water molecules. For the ZnGO sample, similar bands are visible as those for ZnOH, but with a less intensity of the out-of-planes bending and vibration modes of the OH groups. The small bands in the region between 620 and 660 cm^{-1} are linked to the vibrations of CC and C—H bonds of the carbonaceous phase. The bands associated to C—O, C=O bonds in carboxylic and epoxide groups of graphite oxide (GO) were not detected [53,54]. This is another indication that these oxygen functionalities participated in the formation of bonds with the metal hydroxide.

For the exhausted samples, broad groups of new bands appear in various regions of the spectra. A summary of the formed products

Table 3
Assignment of bands detected on FTIR spectra after adsorption of CEES on ZnOH and ZnGO10.

Freq. (cm^{-1})	Vibration mode	Assignment	Ref.
3450	ν(O—H)	(—CH_2OH)	[59,60]
2976	$\nu(CH_2)_{as}$, $\nu(CH_2Cl)_{as}$,	(—C_2H_3), (—CH_2 Cl)	[9,59]
2932	$\nu(CH_3)_{as}$, $\nu(CH_2S)_{as}$,	(—C_2H_4), (—CH_2S)	[9,59]
2886	$\nu(CH_2)_s$, $\nu(CH_2Cl)_s$, $\nu(CH_2S)_s$,	(—CH_2S), (—CH_2Cl)	[9,59]
1613	ν(C=C)	(—CH=CH2)	[45,61]
1453	$\delta(CH_3)_{as}$ bend, $\delta(CH_2)_s$	(—S—CH_3)	[9,59,62]
1422	$\delta(CH_2)_{as}$ scissor	(—CH_2—S—) or (—C_2H_3)	[9,59]
1383	$\delta(CH_3)_s$ bend	(—S—CH_3)	[9,59]
1267	$\delta(CH_2Cl)_{wag}$, δ(OH) [b]	(—CH_2Cl), (—CH_2OH)	[9,59]
1215	$\delta(CH_2S)_{wag}$	(—CH_2—S—)	[9]
970	$\delta(CH_2)_{wag}$	(=C—H)	[9]

and the vibrational frequencies used to monitor these products are given in details in Table 3. The spectral regions below 1700 cm^{-1} for the exhausted samples contain a complex overlap of stretching and deformation vibrational modes of aliphatic CH_x, standalone or bonded with heteroatoms (sulfur or chloride). The characteristics bands at 2976, 2886, 1453 and 1267 cm^{-1} from the CH_2Cl denote the existence of adsorbed CEES molecules on the surface [9]. The characteristic bands from stretching vibrations of the double C=C bond and CH bond of the monosubstituted alkenes (at 2976, 1613, 1550, 1593 and 900 cm^{-1}) from the vinyl group (C=CH_2) [55] indicate the presence of dehydrohalogenation vinylic products such as ethyl vinyl sulfide (EVS), vinyl vinyl sulfide (VVS) and methyl vinyl sulfide (MVS). The bands at 900 and 700 cm^{-1} show a significant intensity increase and are linked to the vibrations of the disubstituted CH.

The broad intense band located between 3600 and 3200 cm^{-1}, which is attributed to the hydroxyl-stretching mode [56], showed a significant increase in the intensity for the exhausted samples. It can be linked either to the formation of 2-hydroxy ethyl ethyl sulfide (HEES), H_2O or also associated with the hydrogen-bonded molecules to the surface ZnOH groups. Both sulfur and chlorine atoms can act as potential hydrogen-bond acceptor sites. Analogous spectral changes to those showed in FTIR spectra of the exhausted samples, due to the hydrogen-bonded molecules, have been reported for the photocatalytic oxidation of CEES on TiO_2 [8]. Furthermore, the bands at 1422 and 1267 cm^{-1} are attributed to deformation vibrations of the OH in the CH_2OH group [9,57,58]. The absence of bands from the stretching vibration of C=O at the region of ketones and aldehydes (1780–1650 cm^{-1}) [9,57,58] indicates that no ketones, carboxylic acids or esters were formed on the surface. The distinguishable bands of the sulfate groups are also not detected. The analysis of the FTIR spectra for the exhausted samples indicates that CEES, HEES and vinylic products exist on the surface.

Thermal analysis results were used to further evaluate the nature of the degradation products and surface reactivity of our materials. TA & DTG curves measured in helium are presented in Supplementary information (Figure S1). For initial ZnOH, the peak on the DTG curves between 140 and 160 °C is assigned to the removal of the physically adsorbed water and the peak centered at 210 °C to the dehydration of $Zn(OH)_2$. The shoulder at about 450 °C can be attributed to $Zn(OH)_2$ dehydroxylation [39]. In the case of composite, the weight loss patterns revealed the same peaks (centered at 150 and 200 °C), plus one wide peak occurred at over 800 °C, which is assigned to the reduction of zinc oxide to Zn (boiling point 907 °C [63]) by the carbonaceous phase.

For both exhausted samples after 7 days of exposure to CEES vapors, the increased weight loss up to 180 °C is related to the removal of water molecules and to the large amount of the degradation products of lower boiling points than that of CEES, such as MVS (b.p. 86 °C), VVS (b.p. 78–92 °C) and EVS (b.p. 92–97 °C) [63]. Physically adsorbed CEES and HEES with boiling points of 156 °C and

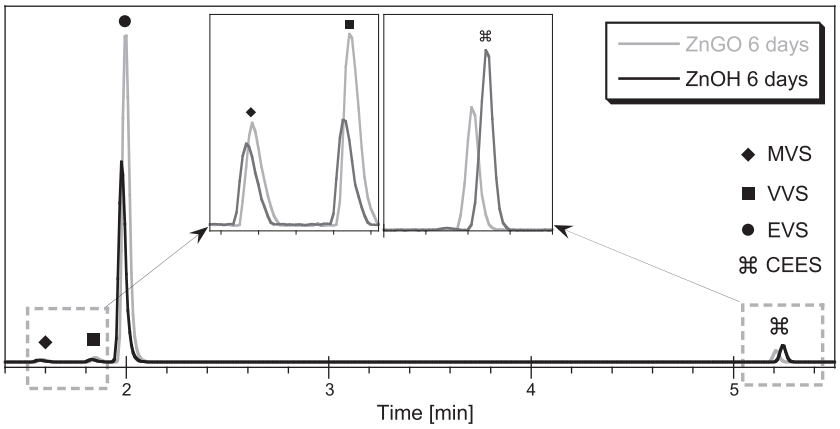

Fig. 5. Chromatograms of the headspace for ZnOH and ZnGO10 after 6 days of CEES exposure.

184 °C [63], respectively, were removed from the pores at the temperature range around 210 °C. Moreover, the new peak that appears for both samples at 460 °C can be assigned to the decomposition of the new surface products such as ZnS, $ZnCl_2$ and $ZnSO_4$ [39]. The existence of new products after the thermal analysis test can be supported by the color change of the samples. The exhausted ZnGO sample after 7 days exposure was grey before the TA test, but it turned yellow (Fig. S2) after the test. The initial material did not change the color after the thermal analysis test.

To further analyze the surface compounds and to determine the byproduct of the decomposition of the mustard gas surrogate on the surface, the extracts from the exhausted samples exposed to CEES were analyzed by MS–MS. The compounds detected on both samples were EVS, HEES and CEES. No traces of VVS, MVS or any oxidation product (diethyl sulfoxide, diethyl sulfone or diethyl sulfone) were found. This does not preclude their presence in the headspace in a non-adsorbed form.

Even though the mass uptakes are helping to evaluate the adsorption performance of the materials, in solitary they cannot provide sufficient evidence about the photocatalytic activities. The results suggest that the interactions of CEES vapors with the surface lead to its photodegradation. It is possible that the products of these reactions do not remain on the surface, especially if they are of high volatility. In this case, the monitoring of the mass increase is not providing enough information on the possible photocatalytic performance. In order to quantify the amount of CEES present in the reaction vessel and to detect the volatile species retained in the gas phase, GC–MS analysis of the headspace vapors/gases was carried out. The results indicated that the amount of CEES in the headspace of the reaction vessel significantly decreased. EVS, VVS and MVS were detected in the headspace as a result of adsorption/transformations of CEES. Interestingly, VVS and MVS were not found in the acetonitrile extracts from the surface. The chromatogram of headspace vapors being in contact with ZnGO10 for 6 days shows that the intensities of the peaks assigned to EVS, VVS and MVS are higher than those detected on the chromatogram of the vapors in contact with ZnOH (Fig. 5). The same trend was found for the samples exposed to CEES for all time periods. We link this increment to the enhanced photoactivity of ZnGO10. The increase of the performance with the addition of the GO can be caused by the alteration in the surface and chemical heterogeneity of the composite. The increased amount and the higher dispersion of the hydroxyl groups as well as the developed porosity play a key role.

The most intense peak of EVS on the chromatograms of the headspace vapors supports the findings from the MS–MS analysis of the extracts, indicating that the degradation of CEES leads mainly to the dehydrohalogenation product. HEES was not detected

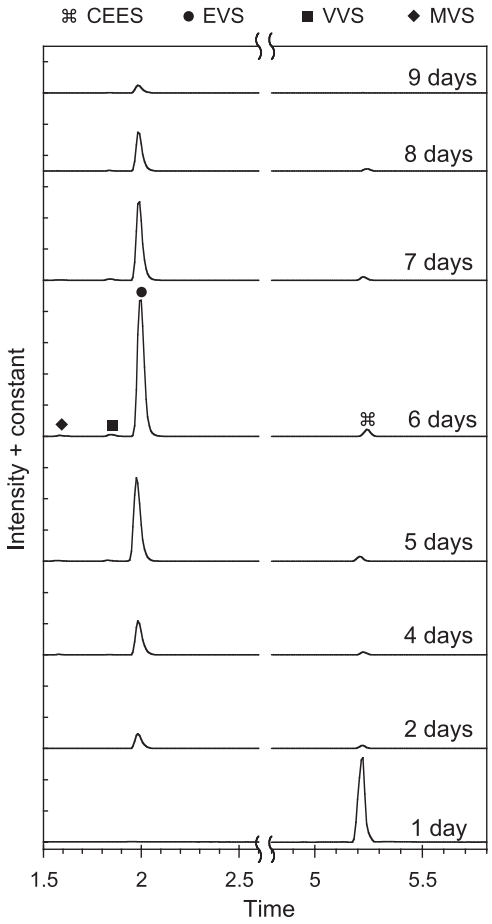

Fig. 6. Tracking of the progress of adsorption and reactions by monitoring chromatograms of ZnGO10 for up to 9 days.

in the headspace. It is likely owing to the fact that its boiling point is 180–184 °C therefore it might be only retained on the surface. We present the comparison of the chromatograms after 6 days of adsorption, since, as it was aforementioned, after seven days vapors started to condense on the surface of ZnOH.

The chromatograms of the headspace for ZnGO10 and the peak areas of every compound detected in the headspace for up to nine days are presented in Figs. 6 and 7, respectively. After a day, the only visible peak is the one linked to CEES. The absence of other peaks is not precluding the formation of the byproducts in the headspace. On the contrary, MS–MS and TA–MS results indicated

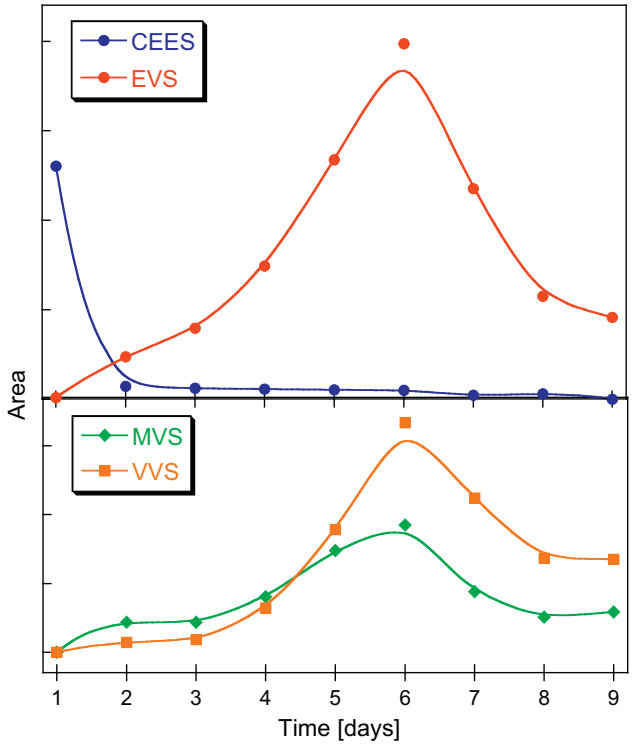

Fig. 7. Dependence of the area of the chromatographic peak (analysis of the headspace) for the particular compounds on the exposure time for ZnGO10.

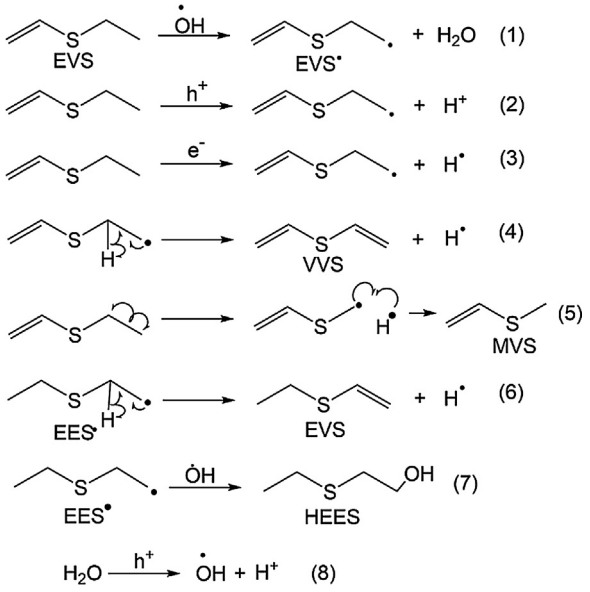

Fig. 8. Schematic representation of the radical reactions.

that EVS and HEES were formed even after a day of exposure. We hypothesize that this inability of detections at the headspace is due to the retention of these byproducts in the pores of the absorbents. The disappearance of CEES and the increase of the EVS, VVS and MVS signals until the sixth day show the on-going photocatalytic transformations of CEES. After the seventh day, the peaks representing the degradation products decrease in their intensity. We link this to the initiation of the vapor condensation on the surface of the samples. The above findings support the conclusion that the samples are acting as photocatalysts, until their surface is saturated with CEES and/or with the formed compounds. Finally, it is important to mention that after 8th day, liquid CEES totally evaporated from the container in the reaction vessel of ZnGO10.

The chromatogram of ZnGO10 shows that after the ninth day of exposure no CEES was detected in the headspace and only EVS, VVS and MVS remained there. The entire amount of CEES either retained on the surface of the samples or degraded. Taking into account the weight increase of the exhausted samples and the density of CEES (d_{CEES} = 1.06 g/mL), the amount of the surrogate that retained or decomposed on the surface after 9 days was 58 wt% on ZnGO10. The rest 42% was totally degraded. Moreover, our composite has the ability for detoxification of the amount of CEES that exceeds twice of its mass. On the other hand, ZnOH did not detoxify the entire CEES, since at the headspace after 9 days of exposure, CEES was still detected. Even though the weight increase of ZnOH was higher than that for ZnGO10, its performance for vapor degradation was worse. The major factor affecting this performance is the condensation of CEES on the surface, limiting the interactions of the surface active sites with the vapors. The adsorption test was carried out also on the pure GO under light or in the dark for up to nine days. The analysis of the headspace and the extracts from the exhausted materials did not reveal any formation of the degradation products.

The degradation pathways of CEES to the less toxic EVS and HEES on ZnO and $Zn(OH)_2$ after 24 h of exposure have been thoroughly reviewed and analyzed in our previous work [20]. Briefly, the formation of the dehydrohalogenation vinylic product, EVS, takes place via a bimolecular elimination (E2) pathway. Adsorbed CEES is transformed to ethyl ethyl sulfonium cation and through an intermolecular cyclization process it is converted to a cyclic cation. A negative charged lattice oxygen of the zinc hydroxide phase, which acts like a Lewis base, accepts labile hydrogen from the cation. Simultaneously, a zinc atom reacts with the produced chloride anion to form zinc chloride. This pathway is promoted by photoexcitation of the material. An electron is excited from the valence to the conduction band of the zinc hydroxide phase by the absorption of a photon, leading to the formation of an electron-hole pair. The width of the band gap indicates the activity in the visible range. It has been shown previously that the addition of graphene phase decreases a band gap in these materials [24]. Moreover, the graphene phase when containing oxygen groups can also provide the photoactivity in the visible range [64–66]. The formed electron/hole pair leads to the formation of hydroxyl radicals [14] and simultaneously forms a transient radical from the destabilization of CEES. This transient radical can react with a hydroxyl radical, forming HEES or it can cause the cleavage of C—S and/or CC bond. Transient radicals can be also formed from the destabilization of the earlier produced EVS.

The unique discovery at the reactive adsorption of CEES on our composites, except the total detoxification of the CEES vapors in a closed system, is the detection of VVS and MVS in the headspace by GC–MS. The formation of these compounds is stimulated by the high photo-reactivity of the surface that promotes further radicals' reaction of the formed EVS. The surface of the composite exhibits a high efficiency for the photodecomposition of CEES and GO seems to increase the efficiency of an electron transfer owing to its electrical conductivity.

Herein, the intention is to describe in more details the contribution of the radical reactions to the catalytic formation of VVS, MVS, EVS and HEES. The hydroxyl radicals, the photogenerated holes in the valence band and the photogenerated electrons at the covalence band play a crucial role in the photochemical destruction of CEES by attacking the formed EVS, following the reactions schematically shown in Fig. 8(1–3).

The presence of water during the adsorption is a constant source of hydroxyl anions that are transformed to hydroxyl radicals when reacting with the holes (Fig. 8, reaction 8). It is also possible that water molecules condense on the surface contribut-

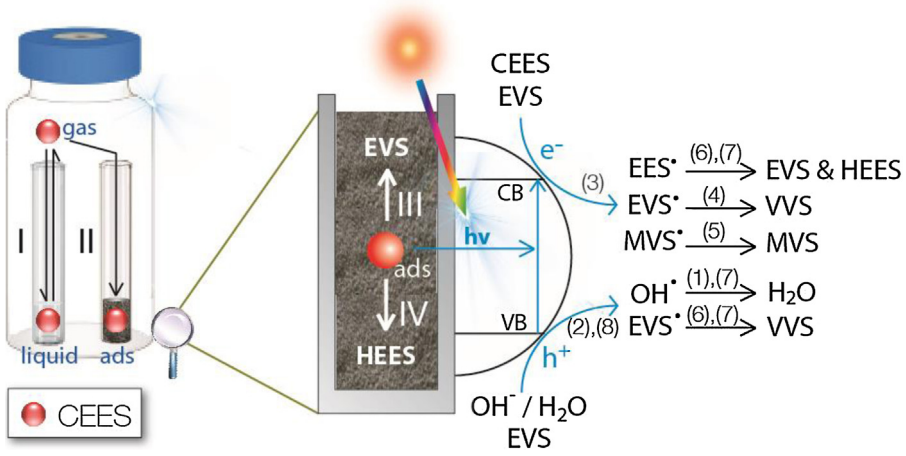

Fig. 9. Schematic representation of all interactions inside the closed adsorption vessel.

ing to an increase in the radical population. This may be linked to the observed gel-like state of the absorbents after seven days of exposure in the case of ZnOH and after eight days for ZnGO10. Moreover, water formation is confirmed by the intense bands on the FTIR spectra of the exhausted materials as well as by the marked weight loss at the temperature less than 100 °C (for the exhausted materials) seen on the TA curves.

The thiol radical (EVS•) can undergo elimination to form VVS by the creation of a vinylic bond (Fig. 8, reaction 4) or to form MVS through the cleavage of the C—C bond (Fig. 8, reaction 5). The "fish-hook" half arrows in Fig. 8 indicate the transfer of a single electron. The formation of EVS can also occur through an intermolecular radical pathway of the produced ethyl ethyl sulfide radical from the adsorption of a photo-exited electron (Fig. 8, reaction 6). Sulfides may also undergo the cleavage of S—C bonds (two in CEES molecule) resulting in various radicals [59]. These radicals can recombine forming disulfides, which are toxic. This pathway took place in the case of the photocatalytic oxidation of CEES on TiO_2 [14]. Disulfides were not detected on the surface or at the headspace of our samples by any of the analytical techniques in this study.

A schematic representation of the reaction pathways is proposed based on the obtained results (Fig. 9). Since in the studied adsorption system the surrogate does not directly interact as a liquid with a solid, the first step of the degradation process is its evaporation from the liquid phase to the gas phase (Fig. 9I). CEES vapors interact then on the surface of our absorbents (Fig. 9II). How fast the equilibrium is reached in Step I and Step II plays a significant role in the reactive adsorption process. The adsorbed CEES undergoes the abovementioned reactions leading to four photocatalytic degradation products (EVS, HEES, MVS and VVS), which are less toxic than is CEES or are non-toxic.

4. Conclusions

The results presented in this paper show that the composites of zinc hydroxide and graphite oxide are more reactive toward CEES degradation than is pure zinc hydroxide. The extent of surface features alterations as well as the adsorption performances strongly depend on the amount of the carbonaceous phase in the composite. Our study indicates that 10% GO is the optimal amount. The significantly higher adsorption capacities in visible light compared to those measured in the dark support the existence of the photocatalytic reactivity. The amount of the terminal OH groups and the extent of the surface area were the most important features governing the adsorption after 24 h of CEES exposure. The increased surface area of the composite promoted the dispersive interactions of the organic molecules with the active sites of the adsorbents. The higher density of the OH groups enhanced the reactivity.

The addition of GO increased the vapor adsorption capacities and the efficiency of the CEES degradation. It was due to an increase in the surface amorphicity level, the chemical heterogeneity and the dispersion of the active inorganic phase. Moreover, GO promoted the formation of active radicals and helped with an electron transfer. After nine days, the composite with 10 % GO retained and/or decomposed the entire amount of CEES introduced to the system, which exceeds more than twice the mass of the composite. The photocatalytic detoxification ability is a unique property, especially taking into account the low cost and the easy synthesis of the composite. Finally, the formed compounds are less toxic or non-toxic which is an important feature of an effective decontamination process.

Acknowledgments

This study was supported by the ARO of USA (Army Research Office), grant W911NF-13-1-0225 and NSF collaborative SBET Grant No. 1133112.

Appendix A. Supplementary data

Supplementary data associated with this article can be found, in the online version, at http://dx.doi.org/10.1016/j.apcatb.2015.10.014.

References

[1] T.C. Marrs, R.L. Maynard, F.R. Sidell, Chemical Warfare Agents: Toxicology and Treatment, 2nd ed., John Wiley & Sons Ltd., New York, 2007.
[2] A. Zawadski, S. Parsons, Acta Crystallogr. E 60 (2004) 225.
[3] K. Kim, O. Tsay, D. Atwood, D. Churchill, Chem. Rev. 111 (2011) 5345.
[4] E. Evgenidou, I. Konstantinou, K. Fytianos, I. Poulios, T. Albanis, Catal. Today 124 (2007) 156.
[5] M.B. Mitchell, V.N. Sheinker, E.A. Mintz, J. Phys. Chem. B 101 (1997) 11192.
[6] V. Sarathy, A.J. Salter, J.T. Nurmi, G. O'Brien Johnson, R.L. Johnson, P.G. Tratnyek, Environ. Sci. Technol. 44 (2010) 787.
[7] B. Singh, T.H. Mahato, A.K. Srivastava, G.K. Prasad, K. Ganesan, R. Vijayaraghavan, R. Jain, J. Hazard. Mater. 190 (2011) 1053.
[8] T.L. Thompson, D.A. Panayotov, J.T. Yates, I. Martyanov, K. Klabunde, J. Phys. Chem. B 108 (2004) 17857.
[9] A.V. Vorontsov, C. Lion, E.N. Savinov, P.G. Smirniotis, J. Catal. 220 (2003) 414.
[10] N. Sharma, R. Kakkar, Adv. Mater. Lett. 4 (2013) 508.
[11] G.W. Peterson, G.W. Wagner, J.H. Keller, J.A. Rossin, Ind. Eng. Chem. Res. 49 (2010) 11182.
[12] G.W. Wagner, O.B. Koper, E. Lucas, S. Decker, K.J. Klabunde, J. Phys. Chem. B 104 (2000) 5118.
[13] G.W. Wagner, L.R. Procell, R.J. O'Connor, M. Shekar, C.L. Carnes, P.N. Kapoor, K.J. Klabunde, J. Am. Chem. Soc. 123 (2001) 1636.

[14] I.N. Martyanov, K.J. Klabunde, Environ. Sci. Technol. 37 (2003) 3448.
[15] G.K. Prasad, T.H. Mahato, B. Singh, K. Ganesan, P. Pandey, K. Sekhar, J. Hazard. Mater. 149 (2007) 460.
[16] D.B. Mawhinney, J.A. Rossin, K. Gerhart, J.T. Yates Jr., Langmuir 15 (1999) 4789.
[17] D.B. Mawhinney, J.A. Rossin, K. Gerhart, J.T. Yates Jr., Langmuir 16 (2000) 2237.
[18] A.-T. Vu, K. Ho, C.H. Lee, Chem. Eng. J. 283 (2016) 1234.
[19] J.A. Arcibar-Orozco, S. Panettieri, T.J. Bandosz, J. Mater. Chem. A 3 (2015) 17080.
[20] D.A. Giannakoudakis, J.A. Arcibar-Orozco, T.J. Bandosz, Appl. Catal. B: Environ. 174 (2015) 96.
[21] T. Bak, J. Nowotny, M. Rekas, C. Sorrell, Int. J. Hydrog. Energy 27 (2002) 991.
[22] V. Srikant, D.R. Clarke, J. Appl. Phys. 83 (1998) 5447.
[23] Y. Lai, M. Meng, Y. Yu, Appl. Catal. B 100 (2010) 491.
[24] S.M.Z. Islam, T. Gayen, A. Moussawi, L. Shi, M. Seredych, T.J. Bandosz, R. Alfano, Opt. Lett. 38 (2013) 962.
[25] D. Sebők, T. Szabó, I. Dékány, Appl. Surf. Sci. 255 (2009) 6953.
[26] R. Gómez, T. López, E. Ortiz-Islas, J. Navarrete, E. Sánchez, F. Tzompanztzi, X. Bokhimi, J. Mol. Catal. A: Chem. 193 (2003) 217.
[27] R. Ullah, J. Dutta, J. Hazard. Mater. 156 (2008) 194.
[28] E. Evgenidou, K. Fytianos, I. Poulios, Appl. Catal. B: Environ. 59 (2005) 81.
[29] H. Barndõk, D. Hermosilla, C. Han, D.D. Dionysiou, C. Negro, A. Blanco, Appl. Catal. B 180 (2016) 44.
[30] F. Giovannelli, A. Ngo Ndimba, P. Diaz-Chao, M. Motelica-Heino, P.I. Raynal, C. Autret, F. Delorme, Powder Technol. 262 (2014) 203.
[31] L. Yang, L. Xiang, J. Nanomater. 2013 (2013) 1.
[32] P. Li, H. Liu, B. Lu, Y. Wei, J. Phys. Chem. C 114 (2010) 21132.
[33] N.J. Nicholas, G.V. Franks, W.A. Ducker, CrystEngComm 14 (2012) 1232.
[34] S. Gadipelli, Z.X. Guo, Prog. Mater. Sci. 69 (2015) 1.
[35] Y. Liu, D. Yan, Y. Li, Z. Wu, R. Zhuo, S. Li, J. Feng, J. Wang, P. Yan, Z. Geng, Electrochim. Acta 117 (2014) 528.
[36] H.S. Song, M.G. Park, S.J. Kwon, K.B. Yi, E. Croiset, Z. Chen, S.C. Nam, Appl. Surf. Sci. 276 (2013) 646.
[37] M. Florent, T.J. Bandosz, Microporous Mesoporous Mater. 204 (2014) 8.
[38] D.A. Giannakoudakis, T.J. Bandosz, J. Colloid Interface Sci. 436 (2014) 296.
[39] O. Mabayoje, M. Seredych, T.J. Bandosz, Appl. Catal. B: Environ. 132 (2013) 321.
[40] M. Seredych, O. Mabayoje, T.J. Bandosz, Chem. Eng. J. 223 (2013) 442.
[41] V.V. Strelko, N.T. Kartel, I.N. Dukhno, V.S. Kuts, R.B. Clarkson, B.M. Odintsov, Surf. Sci. 548 (2004) 281.
[42] W.S. Hummers, R.E. Offeman, J. Am. Chem. Soc. 80 (1958) 1339.
[43] M. Seredych, O. Mabayoje, T.J. Bandosz, J. Phys. Chem. C 116 (2012) 2527.
[44] J. Jagiello, Langmuir 10 (1994) 2778.
[45] J. Jagiello, T.J. Bandosz, J.A. Schwarz, Carbon 32 (1994) 687.
[46] J. Wang, C. Liu, L. Xiang, J. Nanomater. (2013) 1.
[47] G. Kyzas, N. Travlou, O. Kalogirou, E. Deliyanni, Materials 6 (2013) 1360.
[48] P.W. Schindler, W. Stumm, Acuatic Surface Chemistry, John Wiley & Sons, New York, 1987, pp. 83–110.
[49] M. Seredych, O. Mabayoje, M.M. Koleśnik, V. Krstić, T.J. Bandosz, J. Mater. Chem. 22 (2012) 7970.
[50] M. Seredych, O. Mabayoje, T.J. Bandosz, Langmuir 28 (2012) 1337.
[51] J.A. Arcibar-Orozco, T.J. Bandosz, J. Mater. Chem. A 3 (2015) 220.
[52] Y.S. Ho, G. Mckay, Process Saf. Environ. Prot. 76 (1998) 332.
[53] N.A. Travlou, G.Z. Kyzas, N.K. Lazaridis, E.A. Deliyanni, Chem. Eng. J. 217 (2013) 256.
[54] T. Szabó, E. Tombácz, E. Illés, I. Dékány, Carbon 44 (2006) 537.
[55] A. Svatos, A.B. Attygalle, Anal. Chem. 69 (1997) 1827.
[56] N.A. Travlou, G.Z. Kyzas, N.K. Lazaridis, E.A. Deliyanni, Langmuir 29 (2013) 1657.
[57] G. Socrates, Infrared Characteristic Group Frequencies, Wiley, New York, 1994.
[58] R.C. Weast, M.J. Astle, Handbook of Chemistry and Physics, 62nd ed., CRC, Press, Florida, USA, 1981.
[59] S.C. Stout, S.C. Larsen, V.H. Grassian, Microporous Mesoporous Mater. 100 (2007) 77.
[60] D. Panayotov, J.T. Yates, J. Phys. Chem. B 107 (2003) 10560.
[61] G.Z. Kyzas, N.A. Travlou, E.A. Deliyanni, Colloids Surf. B. Biointerfaces 113 (2014) 467.
[62] D. Panayotov, D. Paul, J. Yates, J. Phys. Chem. B 107 (2003) 10571.
[63] W.M. Haynes, CRC Handbook of Chemistry and Physics, 91st ed., Taylor & Francis, Boca Raton, 2010.
[64] J. Robertson, J. Phys. Rev. Lett. 68 (1992) 220.
[65] M.-L. Theye, V. Paret, Carbon 40 (2002) 1153.
[66] J. Robertson, E.P. O'Reilly, Phys. Rev. B 35 (1987) 2946.